Pore-scale imaging of multiphase flow fluctuations in core-scale samples

Shan Wang[1], Catherine Spurin[2], and Tom Bultreys[1]

[1]Ghent University
[2]Stanford University

March 6, 2023

Abstract

Representative elementary volumes (REVs) are an important concept in studying subsurface multiphase flow at the continuum scale. However, fluctuations in multiphase flow are currently not represented in continuum scale models, and their impact at the REV-scale is unknown. Previous pore-scale imaging studies on these fluctuations were limited to small samples with mm-scale diameters and volumes on the order of ~ 0.5 cm3. Here, we image steady-state co-injection experiments on a one-inch diameter core plug sample, with nearly two orders of magnitude larger volume (21 cm3), while maintaining a pore-scale resolution with X-ray micro-computed tomography. This was done for three total flow rates in a series of drainage fractional flow steps. Our observations differ markedly from those reported for mm-scale samples in two ways: the macroscopic fluid distribution was less ramified at low capillary numbers (Ca) of 10-7; and the volume fraction of intermittency initially increased with increasing Ca (similar to mm-scale observations), but then decreased at Ca of 10-7. Our results suggest that viscous forces may play a role in the cm-scale fluid distribution, even at such low Ca, dampening intermittent pathway flow. A REV study of the fluid saturation showed that this may be missed in smaller-scale samples. Pressure drop measurements suggest that the observed pore-scale fluctuations resulted in non-Darcy like upscaled behavior. Overall, we show the importance of large field-of-view high-resolution imaging to bridge the gap between pore- and continuum-scale multiphase flow studies, in particular of pore-scale fluctuations.

Hosted file

`956926_0_art_file_10730244_rqfx51.docx` available at https://authorea.com/users/539115/articles/626067-pore-scale-imaging-of-multiphase-flow-fluctuations-in-core-scale-samples

Hosted file

`956926_0_supp_10730245_rqfx52.docx` available at https://authorea.com/users/539115/articles/626067-pore-scale-imaging-of-multiphase-flow-fluctuations-in-core-scale-samples

Pore-scale imaging of multiphase flow fluctuations in core-scale samples

Shan Wang[1,2], Catherine Spurin[3] and Tom Bultreys[1,2]

[1]Department of Geology, Pore-Scale Processes in Geomaterials Research (PProGRess), Ghent University, Krijgslaan 281/S8, B-9000, Ghent, Belgium

[2]Centre for X-ray Tomography (UGCT), Ghent University, Proeftuinstraat 86, B-9000, Ghent, Belgium

[3]Department of Energy Science & Engineering, Stanford University, Palo Alto, CA, USA

Corresponding author: Shan Wang (Shan.Wang@UGent.be)

Key Points:

- The observations of fluctuations in multiphase flow on cm-scale sample differ markedly from those reported for mm-scale samples
- Viscous forces may play a role in the cm-scale fluid distribution even at low capillary numbers
- Pore-scale fluctuations can result in non-Darcy like upscaled behavior

Abstract

Representative elementary volumes (REVs) are an important concept in studying subsurface multiphase flow at the continuum scale. However, fluctuations in multiphase flow are currently not represented in continuum scale models, and their impact at the REV-scale is unknown. Previous pore-scale imaging studies on these fluctuations were limited to small samples with mm-scale diameters and volumes on the order of ~ 0.5 cm^3. Here, we image steady-state co-injection experiments on a one-inch diameter core plug sample, with nearly two orders of magnitude larger volume (21 cm^3), while maintaining a pore-scale resolution with X-ray micro-computed tomography. This was done for three total flow rates in a series of drainage fractional flow steps. Our observations differ markedly from those reported for mm-scale samples in two ways: the macroscopic fluid distribution was less ramified at low capillary numbers (*Ca*) of 10^{-7}; and the volume fraction of intermittency initially increased with increasing *Ca* (similar to mm-scale observations), but then decreased at *Ca* of 10^{-7}. Our results suggest that viscous forces may play a role in the cm-scale fluid distribution, even at such low *Ca*, dampening intermittent pathway flow. A REV study of the fluid saturation showed that this may be missed in smaller-scale samples. Pressure drop measurements suggest that the observed pore-scale fluctuations resulted in non-Darcy like upscaled behavior. Overall, we show the importance of large field-of-view high-resolution imaging to bridge the gap between pore- and continuum-scale multiphase flow studies, in particular of pore-scale fluctuations.

1 Introduction

Understanding multiphase flow in geological porous materials is central to the safe storage of CO_2 underground (Jeddizahed & Rostami, 2016; Streit & Hillis, 2004) and successful containment of contaminants in the subsurface (McCarthy, 2018). Complex flow dynamics arise from fluid-fluid and fluid-solid interactions over multiple length and time scales (Bultreys et al., 2016; Krevor et al., 2015; Pentland et al., 2011). The underlying pore-scale physics are considered to be mainly controlled by the competition between capillary forces and viscous forces (Chen et al., 2018; Panda et al., 2019; Spurin et al., 2019b). The ratio of

these two forces expressed by means of the capillary number ($Ca = \mu v/\sigma$) is commonly used to differentiate between flow regimes. In the majority of subsurface porous medium applications, the fluid flow is very slow, resulting in capillary numbers $< 10^{-7}$ (Bultreys, 2016).

At the Darcy scale, multiphase flow in porous media is described using averaged properties such as capillary pressure and relative permeability (Lin et al., 2018; Parker, 1989; Zahasky et al., 2020), ignoring fluctuations at the pore scale. However, recent observations at the pore-scale have shown that complex interface dynamics occur even during so-called 'steady-state' flow, where the average fluid saturation of the system remains constant (Reynolds et al., 2017; Zou et al., 2018). For example, fluid phases can rearrange and periodically disconnect and reconnect in a process called intermittent pathway flow, or intermittency (Gao et al., 2019; Reynolds et al., 2017; Spurin et al., 2019a). This influences the energy dissipation in the system and, therefore, impacts the averaged behavior at larger scales (Rücker et al., 2021). Thus the assumption of static interfaces in quasi-static models or continuum frameworks may not be accurate. These phenomena occur even in capillary dominated flow regimes that are commonly assumed to be quasi-static, especially when the viscosity ratio (i.e. ratio of nonwetting phase viscosity to wetting phase viscosity) of the two fluids is very low, as for liquid-gas flows. Previous studies, in small mm-scale samples found intermittent pathway flow was most common, and important to fluid connectivity, at capillary numbers around 10^{-8} - 10^{-6}, with the percentage of intermittently-occupied pores increasing with capillary number, and heterogeneity of the pore space (Spurin et al., 2019a, 2019b).

However, previous pore-scale observations have been limited to mm-scale samples, as 3D X-ray imaging has a trade-off between sample size and resolution (Cnudde & Boone, 2013). These samples are smaller than the typical representative elementary volume (REV) for multiphase flow, making the upscaling from the pore-scale to the core-scale more difficult (Jackson et al., 2020, Zahasky et al., 2020). It has been hypothesized that intermittency does not average out at the REV-scale based on the analysis of fluctuations in the pressure drop

over the sample (Rücker et al., 2021; Spurin et al., 2022), yet pore-scale variations in the fluid distribution have not been observed and characterized directly in REV-scale samples. As such, it is currently unclear how intermittency impacts REV-scale multiphase flow.

In this study, we use the "High-Energy μCT scanner optimized for Research" (HECTOR) at Ghent University's Center for X-ray Tomography (Masschaele et al., 2013) to study pore-scale intermittent fluid dynamics at the core-scale in a sample that is 25 mm in diameter, with a voxel size of 9.6 μm. This sample size - corresponding to a 1 inch drill bit - is a standard for many (relative) permeability measurements, and is thus the smallest size at which the REV concept is typically assumed to be valid in practical applications.

We conduct a series of steady-state two-phase flow experiments on a Bentheimer sandstone sample. Nitrogen and brine were simultaneously injected into the sample at three different total flow rates, representing capillary numbers from 2.21×10^{-9} to 3.59×10^{-7}. At each total flow rate, the brine fractional flow was decreased while the total flow rate was fixed. The micro-CT images allowed us to identify variations in the pore-scale fluid distribution in a time-averaged sense over the course of the scan time (53 minutes) at each fractional flow step (Gao et al., 2019; Spurin et al., 2021). We first present the observation of fluid distribution based on the micro-CT images in Section 3.1.1, followed by an analysis of the influence of capillary number on intermittent pathway flow (Section 3.1.2). The importance of performing multiphase flow study at core-scale is then illustrated by carrying out the representative elementary volume (REV) analysis in Section 3.2. The investigation of fluid distribution in the 3D pore network is shown in Section 3.3 to further understand the intermittency behavior at the core-scale. Finally, Section 3.4 characterizes the dynamics of the pressure signal, supplementing the imaging data with information at a time resolution at the scale of seconds. Overall, the observations discussed in this paper were markedly different than those previously reported on mm-scale samples. The results provide a link between scales, and will aid future upscaling research.

2 Materials and methods

2.1 Core flooding experiment

We perform core flooding experiments on a cylindrical Bentheimer sandstone core of diameter 25 mm and length 42 mm, nearly two orders of magnitude larger volume than previous experiments looking at intermittency (Figure 1). It is a well-sorted German sandstone that contains > 90% quartz (Peksa et al., 2015). For Bentheimer sandstones, the REV for porosity has been observed to be between 1 and 60 mm^3 (Halisch, 2013; Herring et al., 2013). The absolute permeability of the sample measured with deionized water was 1.71 D. The sample was wrapped by a Viton sleeve and placed in an aluminum flow cell (RS Systems, Norway), which has two injection ports and one outflow port. The flow cell and flow lines were firmly attached to the rotation stage of the micro-CT scanner, avoiding effects of the fluid lines tugging or tangling during the imaging. A differential pressure transducer (Keller PD-33X) was used to monitor the differential pressure over the brine inlet and the outlet of the sample.

Steady-state co-injection experiments were conducted with nitrogen as the non-wetting phase and brine (25 wt% potassium iodine) as the wetting phase. The confining pressure and the back pressure were set to 4000 kPa and 2000 kPa respectively, and kept constant during the experiment. The sample was first scanned in its dry state to obtain the geometrical information of the pore structure, this is referred to as the dry scan. Then, brine was injected through the sample at the set back pressure, and a second high-quality scan was made to confirm that all the air was displaced out of the sample, this is referred to as the brine saturated scan. After that, the nitrogen and brine were injected simultaneously through the two injection lines into the sample at a fixed total volumetric flow rate, while the fractional flow f_w (i.e. the volumetric flow rate of brine over the total flow rate) was decreased in a series of drainage fractional flow step. At each step, a scan was taken when the pressure drop across the sample measured by the differential pressure transducer became stable. In this study, 3 observations were made at the total flow rate of 4 ml/min (for f_w = 0.9, 0.7, 0.5); 5 observations at the total flow rate of 1 ml/min (for f_w = 0.9, 0.7, 0.5, 0.25, 0);

and 5 observations at the total flow rate of 0.2 ml/min (for f_w = 0.9, 0.7, 0.5, 0.25, 0). For convenience, we will refer to the three total flow rate experiments 4 ml/min, 1 ml/min and 0.2 ml/min as experiments H, M and L (high, middle and low flow rate) and note the f_w in subscript to describe the fractional flow at each experiment in the following sections. For example, experiment $L_{0.5}$ represents the two-phase flow experiment at f_w = 0.5 for the Q = 0.2 ml/min experiment.

The capillary number (*Ca*) describes the relative importance of capillary forces to viscous forces, and is commonly used to categorize flow regimes. Here, we used the following expression (Spurin et al., 2019b) to quantify the *Ca* at different fractional flows:

$$Ca = \frac{Q_t}{\sigma\left(\frac{f_w}{\mu_w} + \frac{1-f_w}{\mu_{nw}}\right)} \quad (1)$$

where Q_t is the total flow rate, σ is the interfacial tension, μ is the fluid viscosity for the wetting (w) or non-wetting (nw) phase.

The X-ray imaging was performed with the "High Energy micro-CT Optimized for Research" scanner (HECTOR) at the center for X-ray tomography at Ghent University (UGCT). The X-ray energy and the power were 150 kV and 10 W respectively. 3201 projections with 1 s integration time per radiograph were acquired to obtain each image. The voxel size was 9.6 μm for all images, which was the highest resolution the setup could reach to image the full width of the sample. The Octopus software (Tescan-XRE, Belgium) was used to perform the image reconstruction.

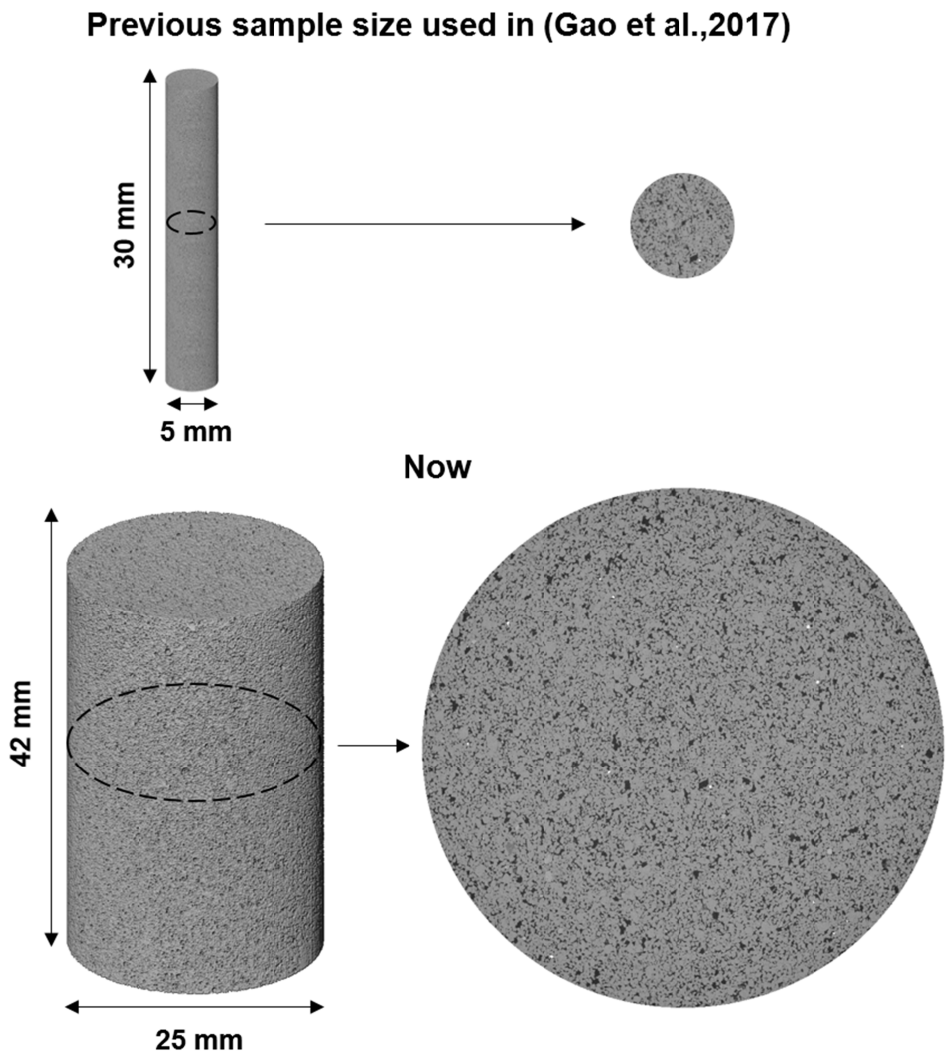

Figure 1. The comparison of sample sizes used in previous experiments (top) and in this study (bottom).

2.2 Image processing

The reconstructed images were registered using normalized mutual information and denoised with a non-local means edge-preserving filter (Buades et al., 2008). To quantify the porosity contributed by macropores (pores clearly resolved at the resolution of the scans) and sub-resolution pores (pores below image resolution), the differential imaging method was used (Gao et al., 2017). The dry scan was first subtracted from the brine saturated scan. Then, the macropores segmented from the filtered dry scan using histogram thresholding were masked out on the differential image and the rest of the fluid-filled phases on

differential image were identified as sub-resolution pores. If we consider the macropore voxels to be 100% porous, while solid grain is 0% porous, the porosity of voxels with sub-resolution pores can be calculated as $\varphi_{sub} = (I_{diff} - CT1)/(CT2 - CT1)$, where I_{diff} is the grey value difference of two images, *CT1* is the threshold value for solid phase, *CT2* is the threshold value for macropores. The detailed procedure can be found in our previous study (Wang et al., 2022). Figure 2(c) shows the porosity distribution map. The total porosity of the sample measured from the differential imaging was 19.58%, with 90% of the total porosity assigned as macropores, the remainder were micropores that could not be resolved with the voxel size of 9.6 μm. This agrees with previously-published results on Bentheimer sandstone (Bultreys et al., 2015). As the sub-resolution microporosity occupies a small percentage of the pore space, and is susceptible to partial volume effects, we focus solely on the fluid distribution in macropores.

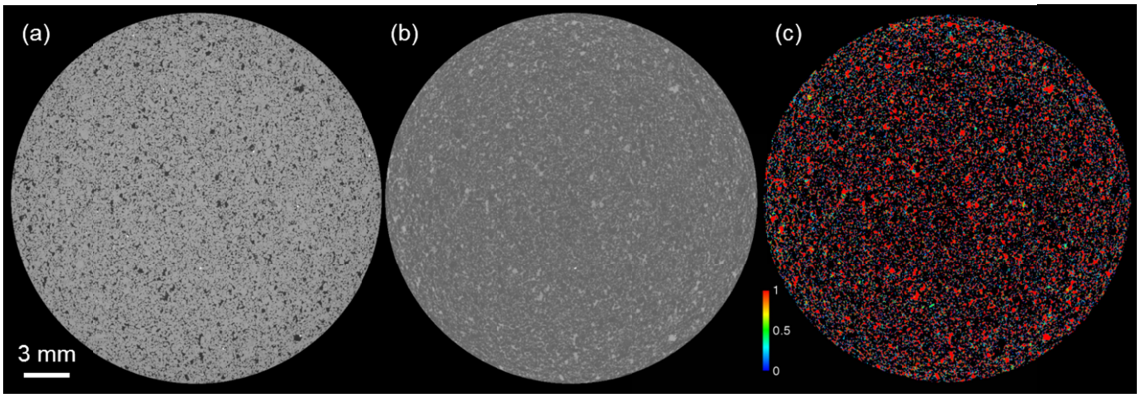

Figure 2. A 2D slice of (a) dry image, (b) brine saturated image and (c) the corresponding porosity distribution map.

As it took approximately 55 minutes to acquire and transfer radiographs for each scan, the fluid distribution in the images reflected time-averaged information. If there was no movement in the sample during the scanning, the pores would be occupied by either nitrogen or brine, presenting as respectively dark or bright gray values in micro-CT images. In case the presence of nitrogen and brine varied periodically in a certain location, this would result in an intermediate gray value, which can be linked to fluid phase intermittency (Spurin et al., 2019a). Similar to the workflow above, the segmentation of nitrogen, brine

and intermittent phases on multiphase scans was also based on the differential imaging method, i.e. the difference image between the brine saturated and the fractional flow scans was used to find the location including both nitrogen and intermittent phases in macropore masked region, then, the nitrogen segmented from the fractional flow scan was subtracted from this image, and the remaining voxels were identified as having intermittent fluid occupancy. To remove partial volume effects that might occur at the fluid-fluid interface, a morphological opening operation (a one-voxel erosion followed by a one-voxel dilation) was performed on the segmented intermittent voxels.

3 Results and discussion

We present the observation of fluid distributions and intermittent pathway flow in the micro-CT images (Section 3.1). The results show that the volume of pore space intermittently occupied by both fluid phases first increases with increasing *Ca*, and then decreases as *Ca* increases further. This differs from a continuously positive correlation between *Ca* number and amount of intermittency observed in mm-scale samples (Spurin et al., 2019b) up to much larger *Ca*. To understand why, we first show the importance of performing multiphase flow studies on core-scale samples by calculating the deterministic REV (dREV) for the nitrogen saturation in Section 3.2. Then the fluid distribution in the 3D pore network is further analyzed to explain the manifestation of intermittent flow pathways at a REV-scale (Section 3.3). We also investigate the pressure fluctuations and discuss the possible relationship between the pressure signal response and the intermittent flow (Section 3.4).

3.1 Observation of the two-phase flow

3.1.1 Fluid distribution in micro-CT images

In our fractional flow experiments, the *Ca* ranges from 2.21×10^{-9} to 3.59×10^{-7}, indicating the system is in the capillary-dominated regime (the threshold of this flow regime is capillary number below $Ca < 10^{-6}$ (Niu et al., 2015)). Our results confirm previous pore-scale studies, which showed the occurrence of intermittency even at capillary numbers

below this threshold.

Figure 3 shows the processed greyscale images for the different fractional flows, with the segmented images shown in Figure 4. For the highest total flow rate experiment (experiment H), the nitrogen mainly invaded the left half of the sample in the beginning, and new flow paths in the right part of the sample were gradually built with decreasing fractional flows, shown in the top panel of Figures 3(a) and 4(a). The fluid distribution for experiments M and L was more ramified, as expected for the case of capillary fingering. In co-injection experiments performed on smaller sandstones or carbonate rock samples (5-6 mm in diameter) by Gao et al. (2020), Lin et al. (2018), Spurin et al. (2021) and Zhang et al. (2021), fluid distributions similar to those in our high flow rate experiment were not reported. One possible reason is that our sample is much larger, the viscous forces at Q = 4 ml/min on the cm-scale start playing a role in the fluid distribution on this scale. If we zoom in on a small part (Figures 3(b) and 4(b)), the distribution may still look like a capillary finger, but globally these fingers are not distributed homogeneously throughout the cross-section of the whole sample, due to viscous forces (Figure 5(a)). Since the total flow rates were lower in the experiments M and L, the capillary effect was stronger. The nonwetting phase therefore generates a ramified fluid distribution like that depicted in Figure 5(b), dominated by the capillary pressure needed to invade individual pore throats (Blunt et al., 1992).

Another observation is the amount of intermittently occupied pore space. As shown in Figure 3, the periodic invasion of nitrogen and brine in specific pores presented intermediate grayscale values in the micro-CT images. Note that the sub-resolution pores also result in voxels with averaged grey values, due to partial volume effects, but these voxels were masked out by the macropore segmentation (as described in Section 2.2). Our image processing workflow thus avoids the erroneous detection of voxels with partial volume effects as containing intermittency. Figure 4. shows the segmentation results of nitrogen, brine and intermittency at different fractional flows.

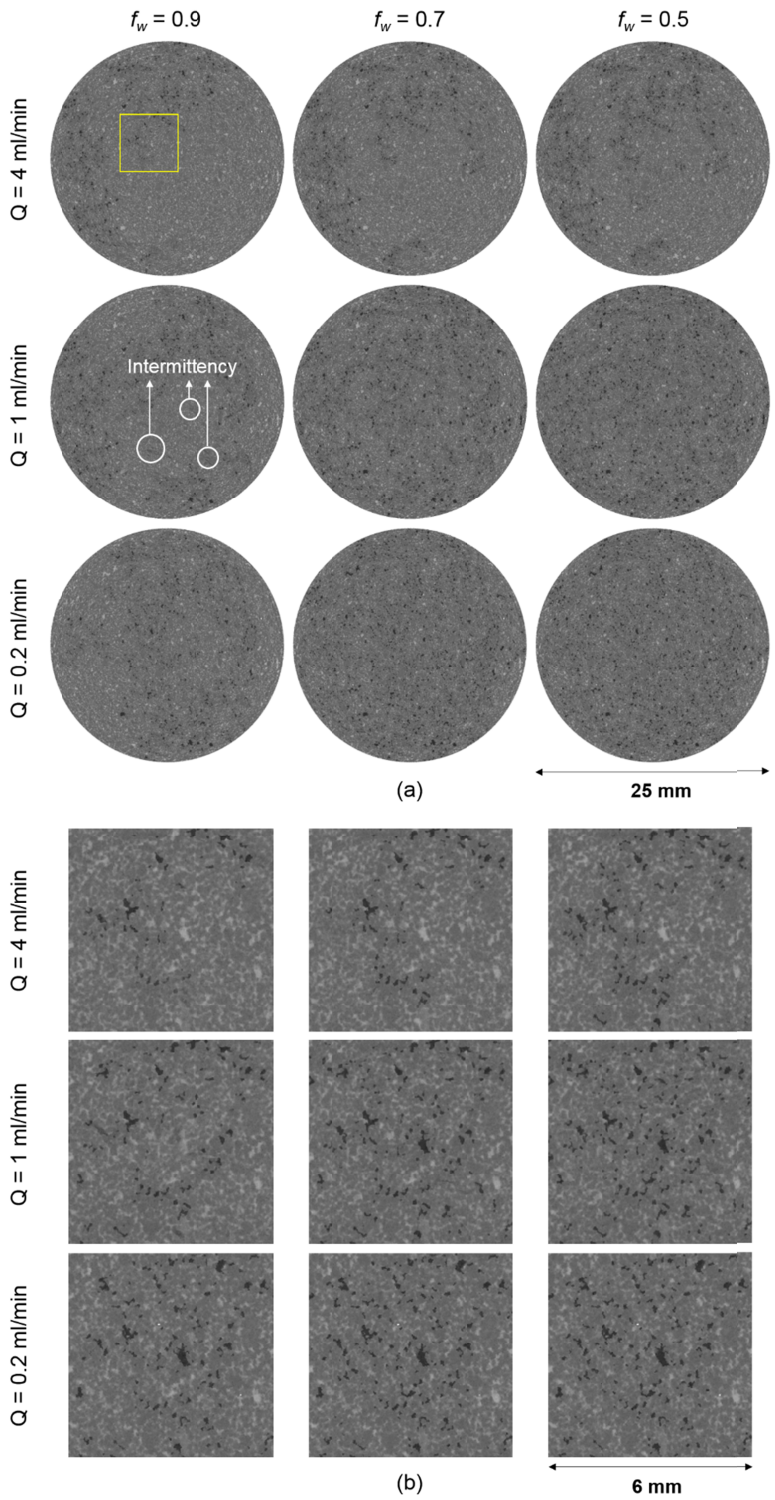

229

230 Figure 3. Greyscale two-dimensional slices of three-dimensional X-ray images at different fractional
231 flows for (a) the whole sample and (b) a zoom in region of the sample for better visibility. The yellow
232 box in the upper left image shows the location of the zoom in region for all images in (a).

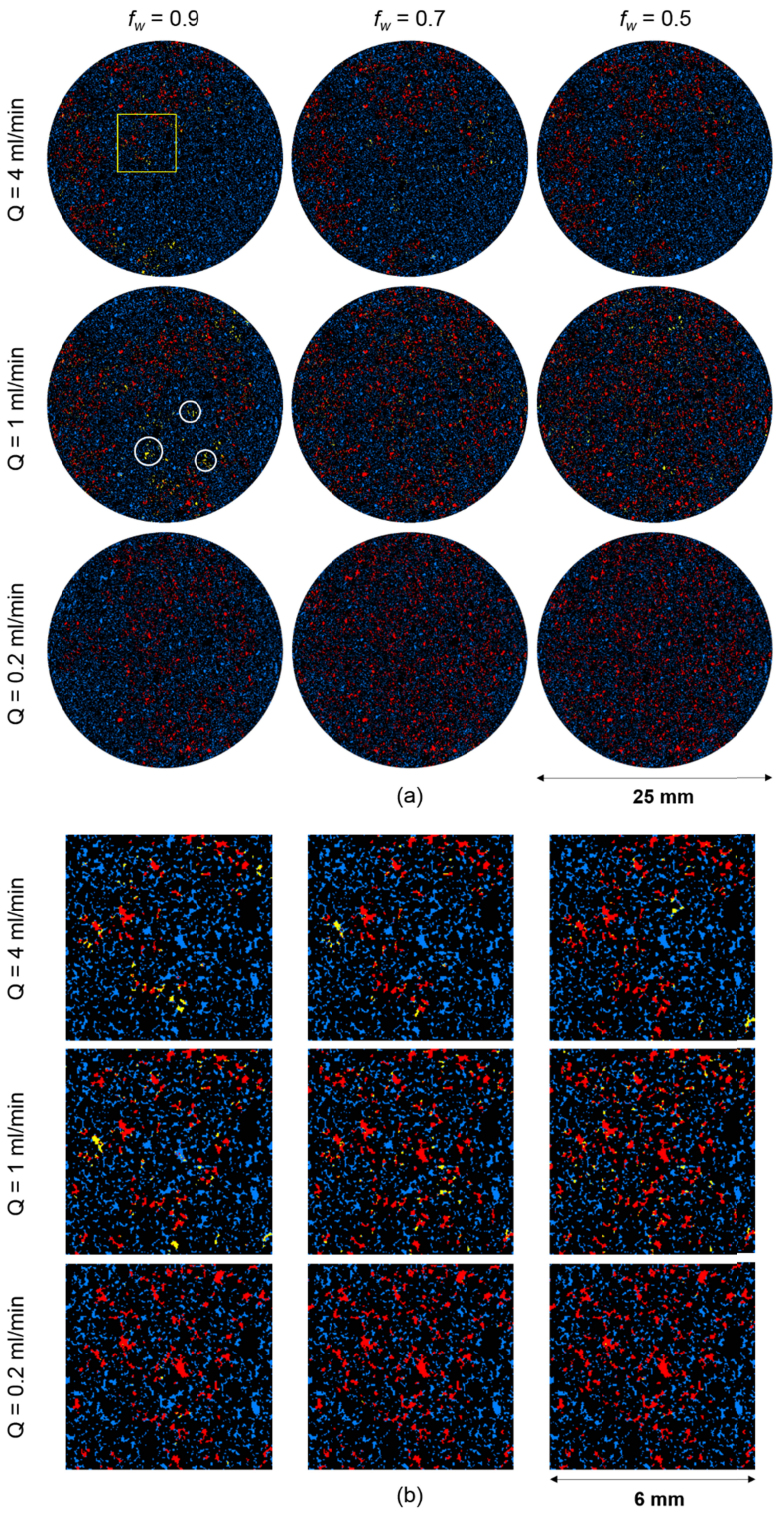

233

234 Figure 4. Segmented images on the same slice as the greyscale images at different fractional flows for (a)
235 the whole sample and (b) a zoom in region of the sample for better visibility. The yellow box in the upper
236 left image shows the location of the zoom in region for all images in (a). The blue, yellow, red and black

represent brine, intermittent phase, nitrogen and solid grain, respectively.

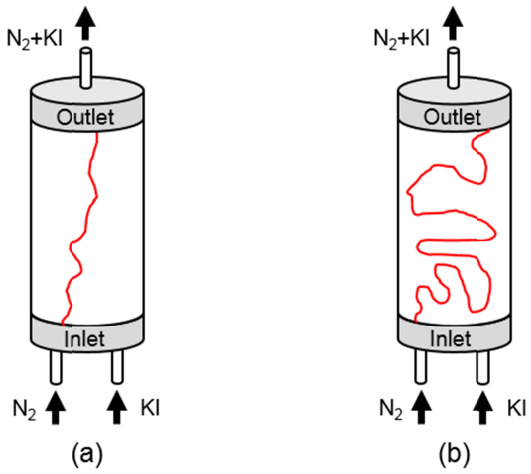

Figure 5. Schematic diagram of typical nitrogen pathways observed in our experiments at (a) high and (b) low flow rate conditions.

3.1.2 Impact of Ca on intermittency

According to the fractional flow experiments performed by Spurin et al. (2021) and Gao et al. (2020) on rock samples with diameters around 5 mm, the percentage of intermittency has a positive correlation with the *Ca* when the latter is of the order 10^{-7} to 10^{-5}, reaching a plateau from 10^{-5} to 10^{-4}. However, despite the similarity of the rock type used, our data did not follow the same trend, due to the variability of the macroscopic saturation distribution in these larger samples.

As shown in Figure 6(a), little intermittency was observed when the *Ca* was lower than 10^{-9}. For the experiments M and L, the capillary forces stabilized the fluid distribution. When the *Ca* increased, the volume fraction of pores being intermittently-occupied at the total flow rate of 1 ml/min was higher than the highest flow rate (4 ml/min) experiment. A possible explanation for the different relationship from mm-scale sample observations is that the brine saturation was relatively high in experiment H (Figure 6(b)), especially in case of f_w = 0.9 which showed highly channeled flow of nitrogen on the left half side of the sample (Figure 7). Intermittent pathway flow could, therefore, only form in limited regions, where

both nitrogen and brine were present. With decreasing f_w, more nitrogen entered the pore space and developed stable pathways, leading the volume of intermittent phase to reduce at f_w = 0.7 and 0.5. In experiment M the brine saturation was lower, and nitrogen was distributed in a more ramified pattern. This causes more opportunity for competition between nitrogen and brine, resulting in more intermittency compared with its highest total flow rate counterpart (Spurin et al., 2021).

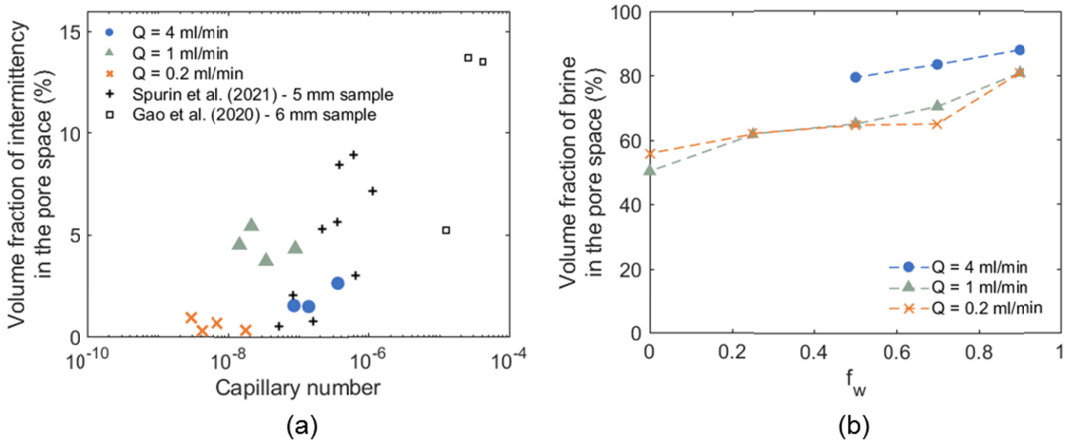

Figure 6. (a) The volume fraction of pores occupied by intermittent phase versus capillary number measured from our 25 mm diameter sample. The results are compared to data obtained on mm-scale experiments (i.e. sample diameter of 5 mm and 6 mm) by Spurin et al. (2021) and Gao et al. (2020). (b) The volume fraction of pores occupied by brine at different fractional flows.

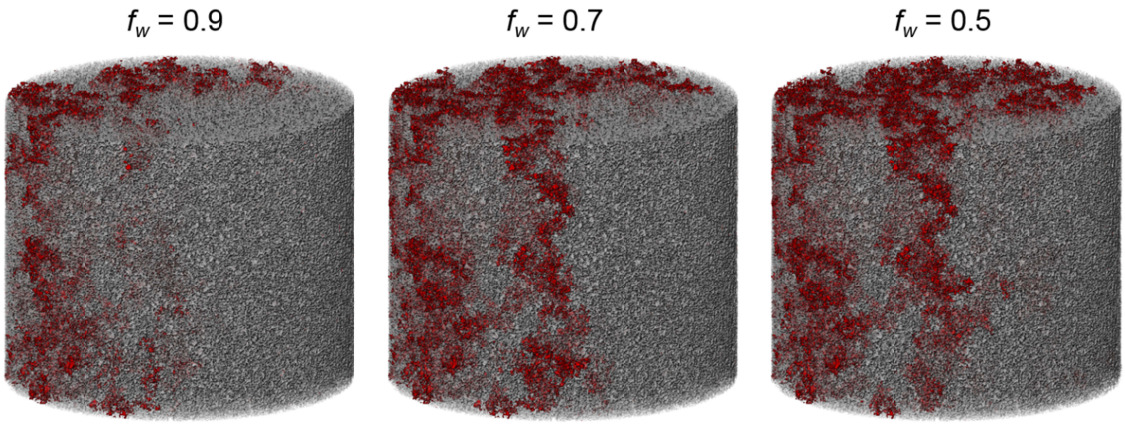

Figure 7. Nitrogen (red) distribution in the 3D pore space (grey) in experiment H. Brine is transparent.

3.2 Representative elementary volume

Linking pore-scale flow behavior to macro-scale or continuum-scale characteristics of porous materials relies on the determination of REV (Singh et al., 2020). A REV is defined as the minimum volume for which the average of a microscopic property first become independent of the averaging volume (Bear, 1972). The size of the REV is not universal and can be different for different properties (e.g. porosity, permeability, saturation, capillary pressure, etc.) of a rock under consideration. In this study, the REV analysis was performed by increasing a cubic domain size from the center of the sample (also called deterministic REV, dREV), calculating the average porosity and nitrogen saturation of the cube calculated at each incremental step. The porosity shows an increasing trend with the cubic volume increasing, and reaches a plateau at around 2 mm linear length (Figure 8(a)). This compares well with the porosity REV size for Bentheimer of >1.75 mm suggested by Halisch (2013) and ≈ 1.25 mm by Jackson et al. (2020). However, the REVs for saturation depend on the flow regime. As seen in Figures 8(b)-8(d), for $Ca < 10^{-7}$ (experiments $H_{0.5}$, M and L), the nitrogen saturation (S_{nw}) continues to slowly decrease even at the largest scale shown, implying that the values of REV exceed the maximum domain size (18 mm) investigated here. This is because the flow paths have a high degree of channeling: if the volume size is increased past the typical cross-sectional size of these channels (past ~ 5-7 mm), the global saturation decreases. The effect may thus go unnoticed in experiments on 5 mm diameter samples. Based on the convergence trend, it appears that for the same fractional flow, a smaller Ca results in a larger REV. In the flow regime for $Ca > 10^{-7}$, the S_{nw} shows less variance for subvolumes larger than 10 mm linear dimension in experiment $H_{0.7}$, indicating that the REV in this regime is approximately 10 mm. This is similar to the observation by Jackson et al. (2020), in which the REV for saturation was larger than the maximum image size (8 mm).

The above analysis indicates that most of the current studies of pore-scale dynamics

(Alhammadi et al., 2020; Gao et al., 2019; Lin et al., 2021; Mascini et al., 2021) on samples with only 5-6 mm diameter are far below the REV requirement for multiphase flow studies. That is why in this study, we use the full image (25 mm diameter) to analyze the fluid performance rather than a cropped region, as this sample size is a standard for many (relative) permeability measurements in the laboratory, and is thus the smallest size at which the REV concept is typically assumed to be valid in real applications.

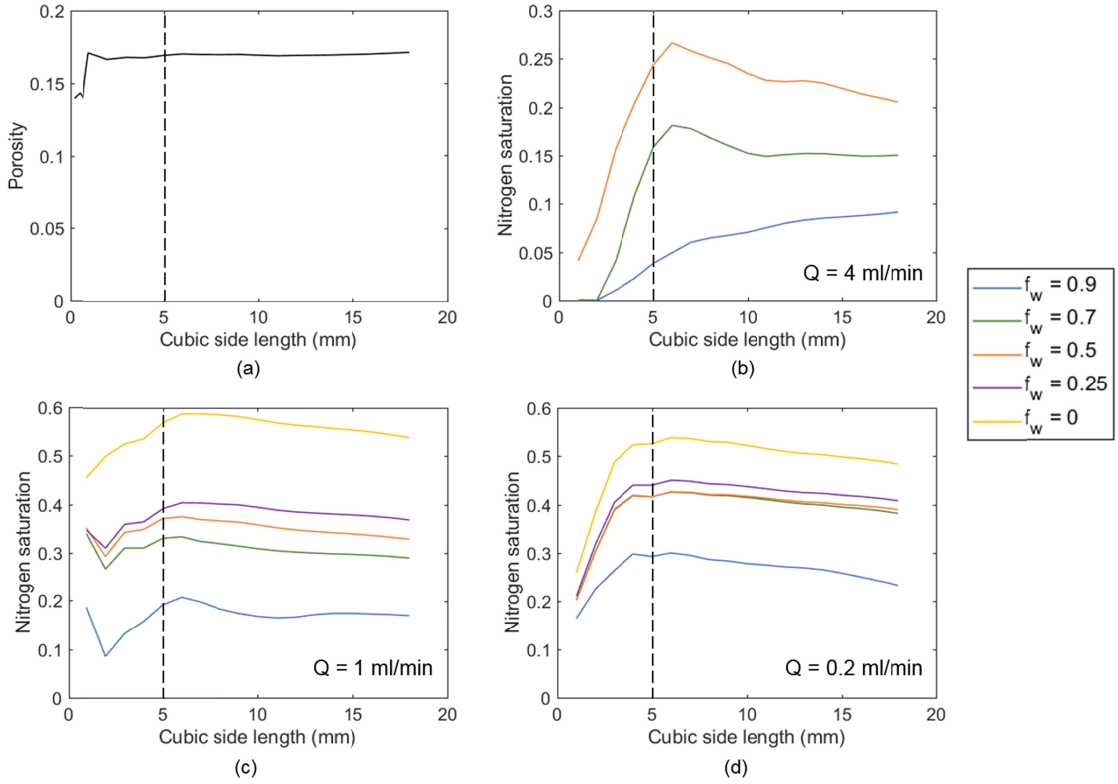

Figure 8. Deterministic REV analysis for (a) porosity and (b)-(d) nitrogen saturation variation in experiments H, M and L. The dotted lines on 5 mm cubic side length show the typical sample size used in previous imaging studies on multiphase flow dynamics in rock samples. This REV study shows that the latter is likely too small to probe the full physical picture.

3.3 Fluid occupancy in the pore network

Intermittent pathway flow provides connections where the non-wetting phase is poorly connected, and could even provide a flow path for otherwise trapped non-wetting phase. This means that it can change the fluid distribution pattern and impact the relative

permeability of fluids. To quantify fluid occupancy in the pore space, a pore network extraction (PNE) algorithm (Raeini et al., 2017) was used to extract and simplify the complex pore morphology into spherical pores (i.e. local dilations in the geometry) connected by throats (i.e. local constrictions in the geometry). The inscribed spheres for the pores were overlaid on the segmented multiphase images to determine which phase (i.e. brine, nitrogen or intermittent fluid) occupied the majority of its voxels. This way, the relationship between pore size and fluid occupancy at each fractional flow step was characterized. As shown in Figure 10, almost all smaller-size pores (< 20 μm) were filled with brine and remained uninvaded. The intermittent phase mainly occupied the intermediate-sized pores (20-40 μm), where the wetting and nonwetting fluids showed more competition. For experiment H (Figure 9(a)), the percentage of nitrogen in pores with 25-45 μm radius showed a notably increase with the decrease of f_w, while that in large pores (>50 μm) was lower than the percentage of brine in all fractional flows. This is contrary to the expectation of capillary-dominated drainage, where the large pores tend to be invaded by the nonwetting fluid first, followed by the invasion of smaller-sized pores due to their correlation with small throats and high entry pressures. This suggests that the fluid invasion behavior is significantly affected by viscous forces, having the effect of causing less intermittency. For experiments M and L (Figures 9(b) and 9(c)), the nitrogen was mainly distributed in pores with 35-45 μm radius. The fraction of nitrogen in large pores (>50 μm) became higher than brine when the f_w was lower than 0.7, indicating that the capillary effect was stronger. This supports our hypothesis that viscous forces are playing an important role in fluid distribution.

Table 1 presents the average coordination numbers (CN) for the pores that remained brine filled, the pores that contained intermittency and the pores that remained nitrogen filled. The coordination measures the number of surrounding pores that are connected via throats to the pore in question. As expected, pores with higher CN are more likely to provide more flow pathways for the invading nitrogen, and are therefore prone to be occupied by nitrogen. Most of the intermittent pores had CN around 4-6 (Figure 10(a)), implying that the

intermittency was favorable in pores with less neighbors. As the brine saturation for experiments $H_{0.5}$, $M_{0.9}$ and $L_{0.9}$ was similar, we compared the CN of intermittent pores and their neighboring pores occupied by different fluids in these three cases (Figure 10(b)). This indicates that the intermittent pores with a large number of CN were likely to be surrounded by brine-filled pores. A possible reason is that if a pore has many neighboring pores and most of them are all filled with nitrogen, they may create a connected flow path directly to perform the displacement. In contrast, if the surrounding pores are brine-filled, they will have more possibilities to reenter the nitrogen-filled pores in a cooperative filling manner, and the intermittent fluid-fluid interface provides the only path for nonwetting fluid to keep the connectivity, which lead to periodic occupancy of both fluids (Spurin et al., 2019a). In addition, Figure 10(b) shows that for the intermittent pores with the same CN, the percentage of nitrogen-occupied neighboring pores in the experiment $M_{0.9}$ case was lower than the other two counterparts, this means that the gas was better connected for the highest and lowest total flow rate cases and there would be fewer potential locations for the water to snap the gas off, which may explain why we observed more intermittency in experiment M.

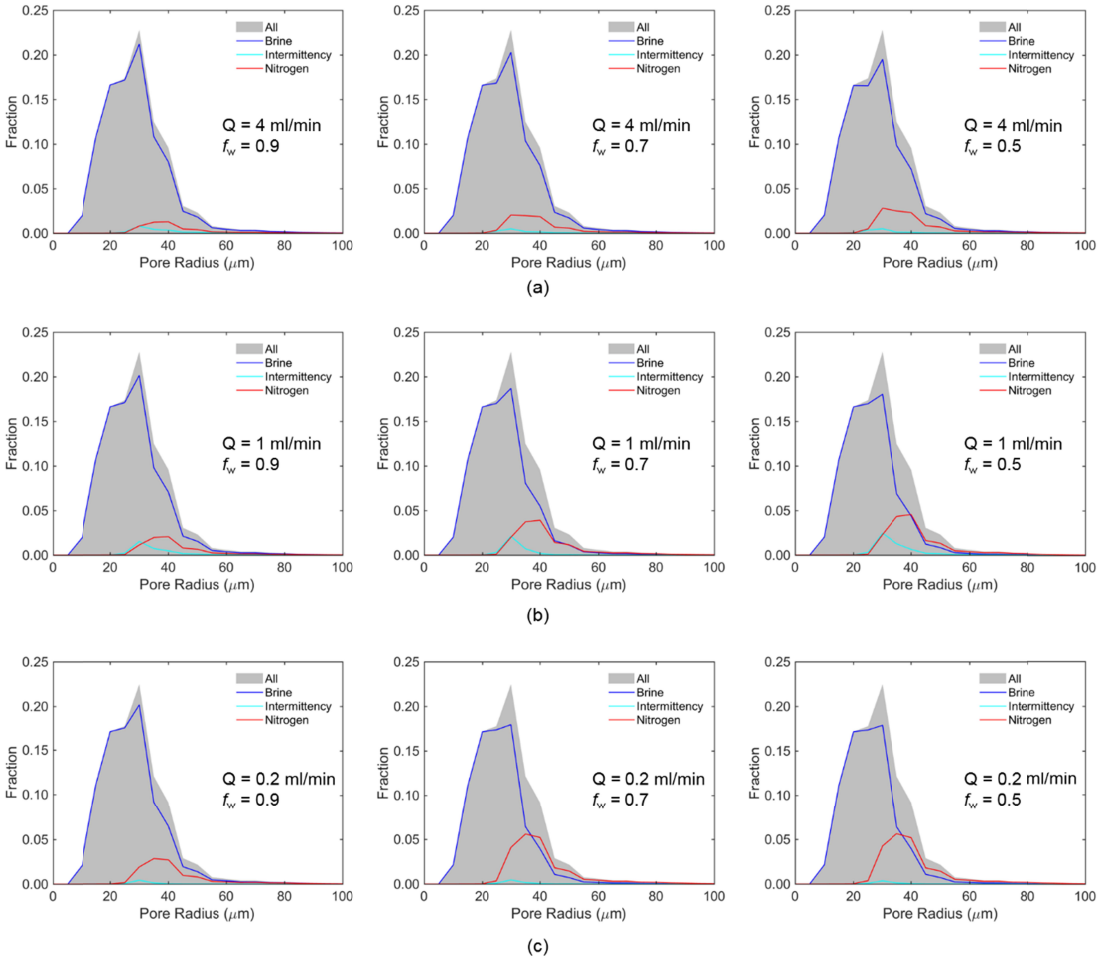

Figure 9. The pore size distribution of different fluid-filling pores in (a) experiment H, (b) experiment M and (c) experiment L. The pore size distribution for all macropores is shown in grey areas, which is obtained from the PNE.

Table 1 Average CN for the brine-filled, intermittency-filled and nitrogen-filled pores during the co-injection process at three total flow rate experiments.

Total flow rate (ml/min)	Brine-filled	Intermittency-filled	Nitrogen-filled
4	3.9	5.6	7.0
1	3.5	5.6	7.3
0.2	3.5	6.0	7.1

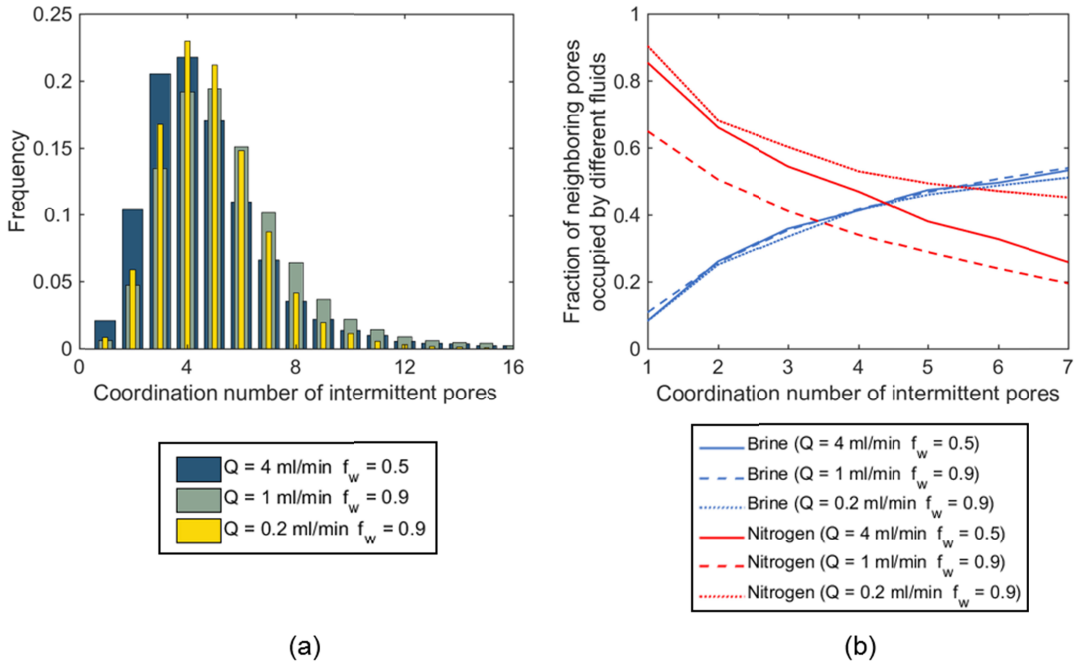

Figure 10. (a) Coordination number distribution of intermittently-occupied pores. (b) The fraction of brine-filled and nitrogen-filled pores surrounding the intermittent pores for different fractional flows. The experiments $H_{0.5}$, $M_{0.9}$ and $L_{0.9}$ are selected because of the similar brine saturation in these three cases.

3.4 Pressure fluctuations in fractional flow experiments

3.4.1 Differential pressure measurements and Darcy's law

Fractional flow experiments typically aim to achieve a "steady-state" at each fractional flow step, which means both the saturation and pressure drop become time-independent. However, clear pressure fluctuations can be found in many fractional flow experiments (Lin et al., 2018; Menke et al., 2022; Spurin et al., 2022; Zou et al., 2018), and also in the experiments presented here. These fluctuations have been shown to be caused by multiphase fluid dynamics, rather than just representing experimental noise (Rucker et al. 2021, Spurin et al. 2022). In this study, the pressure drop over the sample during the co-injection process was measured by a differential pressure transducer, through which we determined whether the system reached the steady state condition (i.e. a stable pressure difference) before each scan was taken. Figure 11 shows the pressure signal during the final 53 minutes of the scan

for each fractional flow.

We first investigate how the measured time-averaged pressure measurements relate to the imposed *Ca,* investigating the meaning of our observations for large-scale modeling of multiphase flow. According to Darcy's law, the *Ca* is proportional to ∇P (i.e. $\nabla P \sim Ca$) in the capillary-dominated regime. This linear relation is known to break down when viscous forces become comparable to capillary forces at a threshold value around $Ca \sim 10^{-3}$ (Blunt, 2017). Recent research has however shown that complex dynamics (e.g. intermittency) that already occur at low *Ca* induce a transition regime for which a power-law relation has been proposed: $\nabla P \sim Ca^a$ (Zhang et al., 2021). This represents a reduction in the resistance to flow compared to Darcy's law, as the fluid distributions (intermittently) change in a way that reduces viscous dissipation. The exponent *a* has been found to be in a range of 0.3 to 0.6, both from theoretical arguments as experimental measurements on small samples and simplified systems (e.g. micromodels and bead packs) (Rassi et al., 2014; Sinha et al., 2017; Tallakstad et al., 2009). Figure 12 shows the measured pressure gradients ∇P as a function of *Ca* for our experiments. While there are only three datapoints for each fractional flow, the curves do appear to show a non-Darcy dependence ($a < 1$), illustrating the relevance of the observed fluctuations towards large-scale simulations. A rough estimate of the exponent *a* from the limited datapoints available is in the range of 0.62 - 0.8, which is higher than values between 0.42 and 0.6 reported for 6 mm diameter Bentheimer samples (Gao et al., 2020; Zhang et al., 2021). The threshold capillary number (Ca^i) for the onset of intermittency derived from Figure 12 is $\sim 10^{-8}$ for $f_w > 0.5$, compared to $\sim 10^{-5}$ in (Gao et al., 2020; Zhang et al., 2021), indicating that the Ca^i for REV-scale sample might be much lower than that defined at the mm-scale. This provides evidence for theoretical analyses on how the effective rheology during multiphase flow scales with length (Roy et al., 2019). Further research with more data points is needed to investigate the results presented here.

Next, we investigate the fluctuations in the pressure signal. The amplitude of these fluctuations was lower in experiment H than in the other experiments, and fluctuations in experiments M and L showed notable periodicity. To differentiate the pressure fluctuations

from noise, the fluctuation histogram is plotted (Figure 13). If the instrumental noise was the main cause of the large fluctuations, this histogram would generally be expected to approximate a Gaussian shape (Rücker et al., 2021). However, in all fractional flows of our experiment, we found non-Gaussian, non-symmetric distributions, implying that the pressure behavior may be a consequence of pore scale displacement events. This leads to the hypothesis that the more pronounced fluctuations in experiment M resulted from the occurrence of more displacement events, confirming the results presented in Figure 6(a): the highest percentage of intermittency was observed under this condition in the imaging. Furthermore, the pressure profile at f_w = 0 was smooth (see the supporting information) since there was no fluid rearrangement in this case, providing further proof that pore-scale fluid rearrangement corresponded to the observed pressure fluctuations. For the lowest total flow rate (experiment L), the pressures were very low (close to 0 kPa) and were less periodic. Comparison to the profile at f_w = 0 implies that the fluid distributions in S were more stable than in the other two cases.

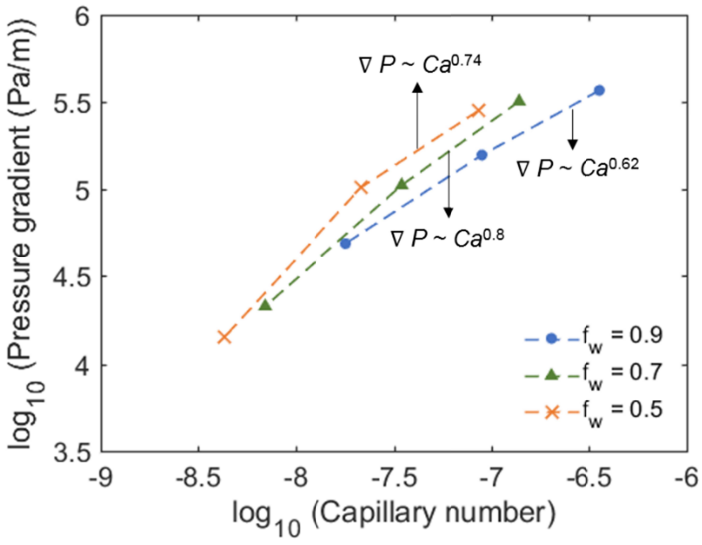

Figure 12. The measured pressure gradients ∇P as a function of Ca at different fractional flows.

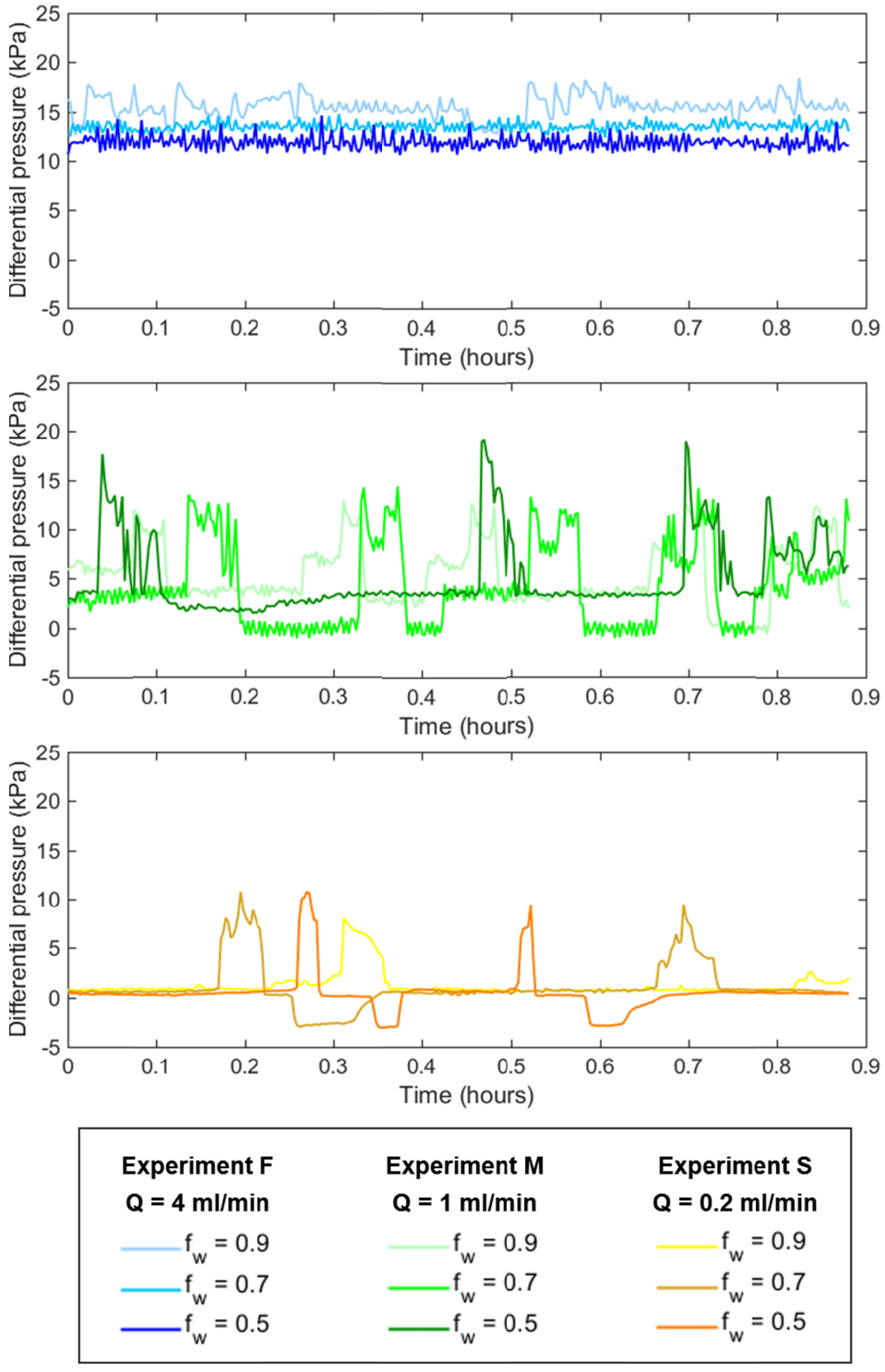

419

420 Figure 11. The differential pressure across the sample measured at steady state during the scan for

421 different fractional flows.

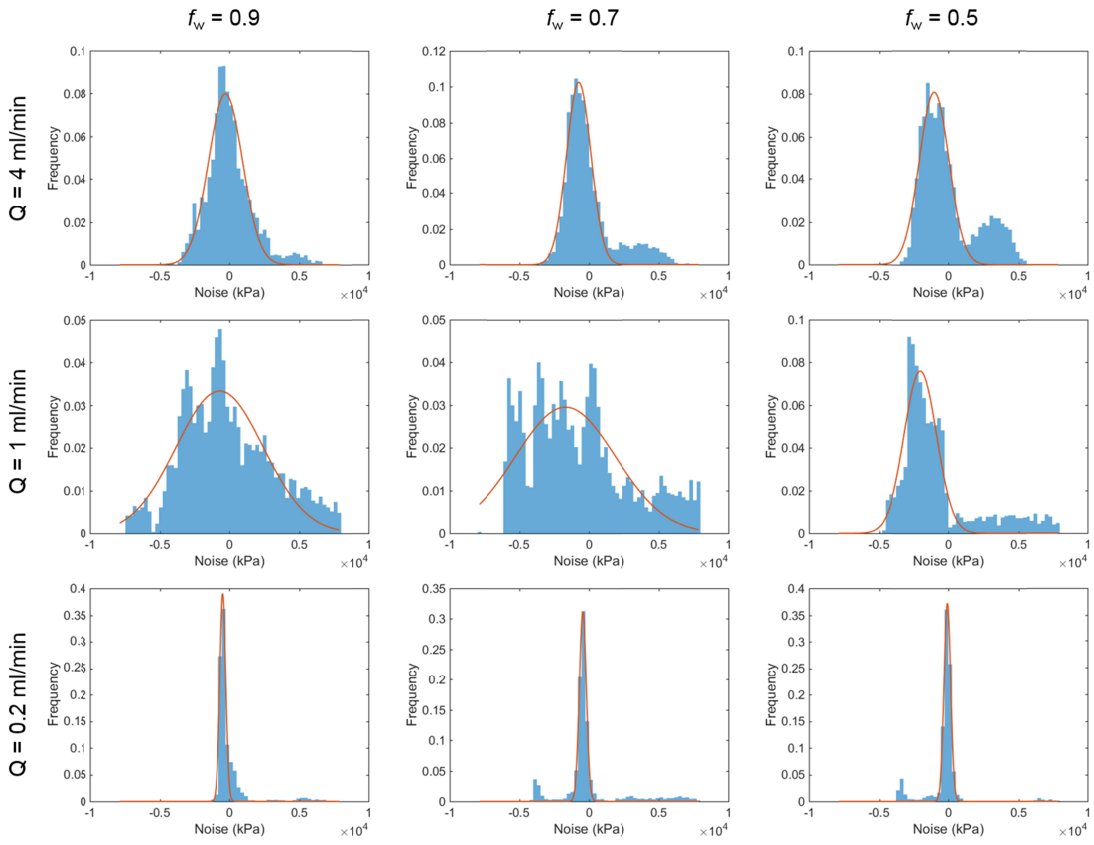

Figure 13. Fluctuation histogram of the pressure signal. A Gaussian fit (orange solid curve) is plotted for comparison with the distribution.

3.4.2 Spectral analysis of pressure data

Here, we analyze the frequency behavior of the pressure fluctuations, thereby supplementing the micro-CT data with higher temporal resolution information. Spurin et al. (2022) observed that fluctuations in differential pressure measurements in a mm-scale carbonate rock sample had the spectral properties of red noise, or $1/f^2$ scaling, by decomposing the pressure data into the frequency domain using a Fourier transformation. This indicates that pressure fluctuations are a stochastic process characterized by self-organized criticality, with no characteristic time or length scale. The scaling relates the power spectral density (S) to the frequency (f):

$$S(f) \sim \frac{1}{f^2} \quad (2)$$

Spurin et al. (2022) asserted that the longest time-scales in this spectrum correspond to repetitive filling of the largest intermittent pores. They showed that the gas connectivity changed for intermittency with a time scale of 8-10 minutes as gas ganglia repeatedly connected and disconnected, while the intermittent gas occupancy with shorter time scales (i.e. 30 s to 2 minutes) were associated with fluctuations without connectivity change, but which may still affect the energy dissipation.

We investigated the spectral properties for our experiments by performing a Fourier transformation on pressure data from the H and M experiments, with the results shown in Figure 14. Experiment L was discounted from this analysis as the pressure drop was small, and close to the resolution of the pressure transducer. As can been seen in Figure 14, the $1/f^2$ scaling (red noise) fitted well for all fractional flow cases in experiment M, where the percentage of intermittently-occupied pores was higher than 3.5%. However, in experiment H, it matched only the $f_w = 0.9$ case, which had an intermittency volume of 2.6%. For $f_w = 0.7$ and 0.5, with intermittency volumes around 1.5%, the power associated to the longer timescales was significantly below red noise scaling, and thus differed from mm-scale observations by Spurin et al. (2022). Since lower frequencies relate to larger sized fluid redistribution events, this may be further evidence for the need to study multiphase dynamics at the core-scale rather than in smaller samples.

For experiment M, the highest amplitudes were at frequencies that correspond to timescales of 10-20 mins. This is the same for $H_{0.9,}$ but for $H_{0.7}$ and $H_{0.5}$ the peak is for timescale of around 20 s. Therefore, we would expect that the intermittently-occupied pores had a large contribution to the non-wetting fluid connectivity in experiment $H_{0.9}$. With the decrease of brine fractional flow, the intermittency may still have played an important role in energy dissipation in experiments $H_{0.7}$ and $H_{0.5}$ – leading to the non-Darcy like behaviour in Figure 12.

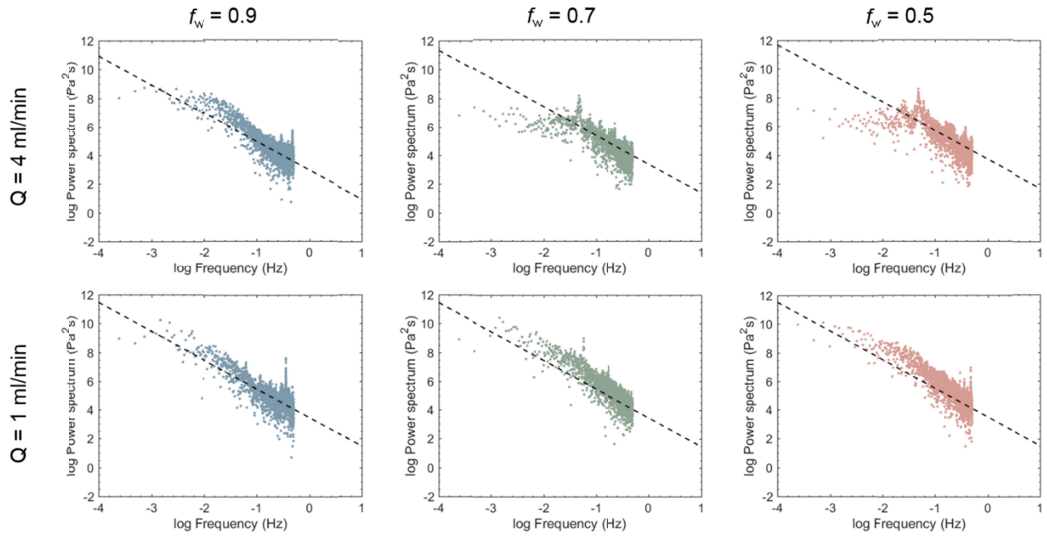

Figure 14. Power spectral density for different fractional flows for Q = 4 ml/min and Q = 1 ml/min. The black dashed line denotes $1/f^2$ scaling.

4 Conclusions

One of the most important challenges in multiphase flow studies is to upscale the fluid dynamics from the pore-scale to the continuum scale. In this work, we observe pore scale dynamics in a core scale sample, assess the upscaled manifestation of these dynamics in the fluid distribution and fluid connectivity, and ultimately link this to the flow resistance reflected by the pressure drop over the sample. At very low *Ca*, we observed the same underlying pore scale dynamics as in small samples. However, at *Ca* on the order of 10^{-7} – traditionally considered to still be well within the capillary-dominated regime – we observed dampening in the amount of intermittent pathway flow. We hypothesize that this is caused by an increased importance of viscous forces, explaining the observation of a less ramified fluid distribution. We show that the latter is difficult to detect on a small sample or a magnified small part of the image. This is reflected in an REV study of the fluid saturation: the saturation varied strongly for averaging volumes with cube sizes up to approximately 10 - 15 mm, after which the variation tailed off but never fully died down to a true constant value reflecting REV.

The analysis of the pressure drop over the sample showed that the observed intermittent

fluid dynamics impact the flow resistance, confirming previous studies that found a non-Darcy-like scaling of the pressure drop with the capillary number, yet finding a larger than expected slope for the $Ca \sim 10^{-7}$ case (i.e. the case with the less ramified distribution). A spectral analysis of the pressure drop showed that the red noise scaling observed in mm-scale samples was only valid for core-scale cases where the percentage of intermittently-occupied pores was relatively high. At higher *Ca*, the spectral slope in our measurements (i.e. experiments $H_{0.7}$ and $H_{0.5}$) became flatter for timescales > 20 s. We suggest that the intermittency may still play an important role in energy dissipation in these two cases, leading to the non-Darcy like behaviour.

Overall, our research shows the need to study pore-scale dynamics in samples that approach the REV scale – or, from a practical point of view, at least the scale at which continuum properties such as capillary pressure and (relative) permeability curves are typically measured, in case a true REV does not exist. However, the limited time resolution of the laboratory-based micro-CT scanner for such samples did not allow us to further track the fluid dynamics at different time scales. Our findings need to be confirmed by more experiments on cm-scale samples with different fluids, rock types, wettability and pore structures. This may provide us a deeper understanding of fluid flow from small scale to large scale, which could be important for the design of secure subsurface storage of carbon dioxide and energy, as well as for ground-water studies.

Acknowledgments

Shan Wang would like to acknowledge the China Scholarship Council (CSC Grant 201906440157) for PhD support. Tom Bultreys holds a senior research fellowship from the Research Foundation-Flanders (FWO) under grant 12X0922N. This work was also partially funded by the FWO (Junior) Research Project program (G051418N and G004820N) and the UGent BOF funding for the Centre of Expertise UGCT (BOF.EXP.2017.0007). Catherine Spurin acknowledges funding from BHP as part of the GeoCquest project. Dr. M. Borji and S. Ellman are thanked for their help with the experimental setup.

References

Alhammadi, A. M., Gao, Y., Akai, T., Blunt, M. J., & Bijeljic, B. (2020). Pore-scale X-ray imaging with measurement of relative permeability, capillary pressure and oil recovery in a mixed-wet micro-porous carbonate reservoir rock. *Fuel*, *268*(January), 117018. https://doi.org/10.1016/j.fuel.2020.117018

Bear, J. (1972). Dynamics of fluids in porous media. Elsevier, New York. *Dynamics of Fluids in Porous Media. Elsevier, New York.*

Blunt, M., King, M. J., & Scher, H. (1992). Simulation and theory of two-phase flow in porous media. *Physical Review A*, *46*(12), 7680–7699. https://doi.org/10.1103/PhysRevA.46.7680

Blunt, M. J. (2017). *Multiphase flow in permeable media: A pore-scale perspective*. Cambridge university press.

Buades, A., Coll, B., & Morel, J. M. (2008). Nonlocal image and movie denoising. *International Journal of Computer Vision*, *76*(2), 123–139. https://doi.org/10.1007/s11263-007-0052-1

Bultreys, T. (2016). *Two-phase flow in rocks: new insights from multi-scale pore network modeling and fast pore scale visualization*. Ghent University.

Bultreys, T., Boone, M. A., Boone, M. N., De Schryver, T., Masschaele, B., Van Loo, D., et al. (2015). Real-time visualization of Haines jumps in sandstone with laboratory-based microcomputed tomography. *Water Resources Research*, *51*(10), 8668–8676. https://doi.org/10.1002/2015WR017502

Bultreys, T., Boone, M. A., Boone, M. N., De Schryver, T., Masschaele, B., Van Hoorebeke, L., & Cnudde, V. (2016). Fast laboratory-based micro-computed tomography for pore-scale research: Illustrative experiments and perspectives on the future. *Advances in Water Resources*, *95*, 341–351. https://doi.org/10.1016/j.advwatres.2015.05.012

Chen, Y. F., Guo, N., Wu, D. S., & Hu, R. (2018). Numerical investigation on immiscible

displacement in 3D rough fracture: Comparison with experiments and the role of viscous and capillary forces. *Advances in Water Resources*, *118*, 39–48. https://doi.org/10.1016/j.advwatres.2018.05.016

Cnudde, V., & Boone, M. N. (2013). High-resolution X-ray computed tomography in geosciences: A review of the current technology and applications. *Earth-Science Reviews*, *123*, 1–17. https://doi.org/10.1016/j.earscirev.2013.04.003

Gao, Y., Lin, Q., Bijeljic, B., & Blunt, M. J. (2017). X-ray Microtomography of Intermittency in Multiphase Flow at Steady State Using a Differential Imaging Method. *Water Resources Research*, *53*(12), 10274–10292. https://doi.org/10.1002/2017WR021736

Gao, Y., Qaseminejad Raeini, A., Blunt, M. J., & Bijeljic, B. (2019). Pore occupancy, relative permeability and flow intermittency measurements using X-ray micro-tomography in a complex carbonate. *Advances in Water Resources*, *129*(April), 56–69. https://doi.org/10.1016/j.advwatres.2019.04.007

Gao, Y., Lin, Q., Bijeljic, B., & Blunt, M. J. (2020). Pore-scale dynamics and the multiphase Darcy law. *Physical Review Fluids*, *5*(1), 13801. https://doi.org/10.1103/PhysRevFluids.5.013801

Halisch, M. (2013). The Rev Challenge – Estimating Representative Elementary Volumes and Porous Rock Inhomogeneity From High Resolution Micro-Ct Data Sets. In *International Symposium of the Society of Core Analysts* (pp. 1–7). Retrieved from http://www.jgmaas.com/SCA/2013/SCA2013-069.pdf

Herring, A. L., Harper, E. J., Andersson, L., Sheppard, A., Bay, B. K., & Wildenschild, D. (2013). Effect of fluid topology on residual nonwetting phase trapping: Implications for geologic CO2 sequestration. *Advances in Water Resources*, *62*, 47–58. https://doi.org/10.1016/j.advwatres.2013.09.015

Jackson, S. J., Lin, Q., & Krevor, S. (2020). Representative Elementary Volumes, Hysteresis, and Heterogeneity in Multiphase Flow From the Pore to Continuum Scale. *Water*

559 *Resources Research*, *56*(6), e2019WR026396. https://doi.org/10.1029/2019WR026396

560 Jackson, Samuel J., Agada, S., Reynolds, C. A., & Krevor, S. (2018). Characterizing
561 Drainage Multiphase Flow in Heterogeneous Sandstones. *Water Resources Research*,
562 *54*(4), 3139–3161. https://doi.org/10.1029/2017WR022282

563 Jeddizahed, J., & Rostami, B. (2016). Experimental investigation of injectivity alteration due
564 to salt precipitation during CO2 sequestration in saline aquifers. *Advances in Water*
565 *Resources*, *96*, 23–33. https://doi.org/10.1016/j.advwatres.2016.06.014

566 Krevor, S., Blunt, M. J., Benson, S. M., Pentland, C. H., Reynolds, C., Al-Menhali, A., & Niu,
567 B. (2015). Capillary trapping for geologic carbon dioxide storage - From pore scale
568 physics to field scale implications. *International Journal of Greenhouse Gas Control*, *40*,
569 221–237. https://doi.org/10.1016/j.ijggc.2015.04.006

570 Lin, Q., Bijeljic, B., Pini, R., Blunt, M. J., & Krevor, S. (2018). Imaging and Measurement of
571 Pore-Scale Interfacial Curvature to Determine Capillary Pressure Simultaneously With
572 Relative Permeability. *Water Resources Research*, *54*(9), 7046–7060.
573 https://doi.org/10.1029/2018WR023214

574 Lin, Q., Bijeljic, B., Foroughi, S., Berg, S., & Blunt, M. J. (2021). Pore-scale imaging of
575 displacement patterns in an altered-wettability carbonate. *Chemical Engineering Science*,
576 *235*, 116464. https://doi.org/10.1016/j.ces.2021.116464

577 Mascini, A., Boone, M., Van Offenwert, S., Wang, S., Cnudde, V., & Bultreys, T. (2021).
578 Fluid Invasion Dynamics in Porous Media With Complex Wettability and Connectivity.
579 *Geophysical Research Letters*, *48*(22), 1–10. https://doi.org/10.1029/2021GL095185

580 Masschaele, B., Dierick, M., Loo, D. Van, Boone, M. N., Brabant, L., Pauwels, E., et al.
581 (2013). HECTOR: A 240kV micro-CT setup optimized for research. In *Journal of*
582 *Physics: Conference Series* (Vol. 463, p. 12012).
583 https://doi.org/10.1088/1742-6596/463/1/012012

584 McCarthy, J. F. (2018). Sampling and characterization of colloids and particles in

groundwater for studying their role in contaminant transport. In *Environmental particles* (pp. 247–315). CRC Press.

Menke, H. P., Gao, Y., Linden, S., & Andrew, M. G. (2022). Using Nano-XRM and High-Contrast Imaging to Inform Micro-Porosity Permeability During Stokes–Brinkman Single and Two-Phase Flow Simulations on Micro-CT Images. *Frontiers in Water*, *4*. https://doi.org/10.3389/frwa.2022.935035

Niu, B., Al-Menhali, A., & Krevor, S. C. (2015). The impact of reservoir conditions on the residual trapping of carbon dioxide in Berea sandstone. *Water Resources Research*, *51*(4), 2009–2029. https://doi.org/10.1002/2014WR016441

Panda, A., Pati, A. R., Saha, B., Kumar, A., & Mohapatra, S. S. (2019). The role of viscous and capillary forces in the prediction of critical conditions defining super-hydrophobic and hydrophilic characteristics. *Chemical Engineering Science*, *207*, 527–541. https://doi.org/10.1016/j.ces.2019.06.013

Parker, J. C. (1989). Multiphase flow and transport in porous media. *Reviews of Geophysics*, *27*(3), 311–328. https://doi.org/10.1029/RG027i003p00311

Peksa, A. E., Wolf, K. H. A. A., & Zitha, P. L. J. (2015). Bentheimer sandstone revisited for experimental purposes. *Marine and Petroleum Geology*, *67*, 701–719. https://doi.org/10.1016/j.marpetgeo.2015.06.001

Pentland, C. H., El-Maghraby, R., Iglauer, S., & Blunt, M. J. (2011). Measurements of the capillary trapping of super-critical carbon dioxide in Berea sandstone. *Geophysical Research Letters*, *38*(6).

Raeini, A. Q., Bijeljic, B., & Blunt, M. J. (2017). Generalized network modeling: Network extraction as a coarse-scale discretization of the void space of porous media. *Physical Review E*, *96*(1), 13312. https://doi.org/10.1103/PhysRevE.96.013312

Rassi, E. M., Codd, S. L., & Seymour, J. D. (2014). Corrigendum: Nuclear magnetic resonance characterization of the stationary dynamics of partially saturated media during

steady-state infiltration flow (2011 New J. Phys. 13 015007). *New Journal of Physics*, *16*(1), 15007. https://doi.org/10.1088/1367-2630/16/3/039501

Reynolds, C. A., Menke, H., Andrew, M., Blunt, M. J., & Krevor, S. (2017). Dynamic fluid connectivity during steady-state multiphase flow in a sandstone. *Proceedings of the National Academy of Sciences of the United States of America*, *114*(31), 8187–8192. https://doi.org/10.1073/pnas.1702834114

Roy, S., Sinha, S., & Hansen, A. (2019). Immiscible two-phase flow in porous media: Effective rheology in the continuum limit. *ArXiv Preprint ArXiv:1912.05248*. Retrieved from http://arxiv.org/abs/1912.05248

Rücker, M., Georgiadis, A., Armstrong, R. T., Ott, H., Brussee, N., van der Linde, H., et al. (2021). The Origin of Non-thermal Fluctuations in Multiphase Flow in Porous Media. *Frontiers in Water*, *3*, 45. https://doi.org/10.3389/frwa.2021.671399

Singh, A., Regenauer-Lieb, K., Walsh, S. D. C., Armstrong, R. T., van Griethuysen, J. J. M., & Mostaghimi, P. (2020). On Representative Elementary Volumes of Grayscale Micro-CT Images of Porous Media. *Geophysical Research Letters*, *47*(15), e2020GL088594. https://doi.org/10.1029/2020GL088594

Sinha, S., Bender, A. T., Danczyk, M., Keepseagle, K., Prather, C. A., Bray, J. M., et al. (2017). Effective Rheology of Two-Phase Flow in Three-Dimensional Porous Media: Experiment and Simulation. *Transport in Porous Media*, *119*(1), 77–94. https://doi.org/10.1007/s11242-017-0874-4

Spurin, C., Bultreys, T., Bijeljic, B., Blunt, M. J., & Krevor, S. (2019a). Intermittent fluid connectivity during two-phase flow in a heterogeneous carbonate rock. *Physical Review E*, *100*(4), 1–10. https://doi.org/10.1103/PhysRevE.100.043103

Spurin, C., Bultreys, T., Bijeljic, B., Blunt, M. J., & Krevor, S. (2019b). Mechanisms controlling fluid breakup and reconnection during two-phase flow in porous media. *Physical Review E*, *100*(4), 1–5. https://doi.org/10.1103/PhysRevE.100.043115

637 Spurin, C., Bultreys, T., Rücker, M., Garfi, G., Schlepütz, C. M., Novak, V., et al. (2021).
638 The development of intermittent multiphase fluid flow pathways through a porous rock.
639 *Advances in Water Resources*, *150*(November 2020), 103868.
640 https://doi.org/10.1016/j.advwatres.2021.103868

641 Spurin, C., Rücker, M., Moura, M., Bultreys, T., Garfi, G., Berg, S., et al. (2022). Red Noise
642 in Steady-State Multiphase Flow in Porous Media. *Water Resources Research*, *58*(7),
643 e2022WR031947. https://doi.org/10.1029/2022WR031947

644 Streit, J. E., & Hillis, R. R. (2004). Estimating fault stability and sustainable fluid pressures
645 for underground storage of CO2 in porous rock. *Energy*, *29*(9–10), 1445–1456.
646 https://doi.org/10.1016/j.energy.2004.03.078

647 Tallakstad, K. T., Knudsen, H. A., Ramstad, T., Løvoll, G., Måløy, K. J., Toussaint, R., &
648 Flekkøy, E. G. (2009). Steady-state two-phase flow in porous media: Statistics and
649 transport properties. *Physical Review Letters*, *102*(7), 74502.
650 https://doi.org/10.1103/PhysRevLett.102.074502

651 Wang, S., Ruspini, L. C., Øren, P. E., Van Offenwert, S., & Bultreys, T. (2022). Anchoring
652 Multi-Scale Models to Micron-Scale Imaging of Multiphase Flow in Rocks. *Water*
653 *Resources Research*, *58*(1), 1–16. https://doi.org/10.1029/2021WR030870

654 Zahasky, C., Jackson, S. J., Lin, Q., & Krevor, S. (2020). Pore Network Model Predictions of
655 Darcy-Scale Multiphase Flow Heterogeneity Validated by Experiments. *Water*
656 *Resources Research*, *56*(6), 1–16. https://doi.org/10.1029/2019WR026708

657 Zhang, Y., Bijeljic, B., Gao, Y., Lin, Q., & Blunt, M. J. (2021). Quantification of Nonlinear
658 Multiphase Flow in Porous Media. *Geophysical Research Letters*, *48*(5).
659 https://doi.org/10.1029/2020GL090477

660 Zou, S., Armstrong, R. T., Arns, J. Y., Arns, C. H., & Hussain, F. (2018). Experimental and
661 Theoretical Evidence for Increased Ganglion Dynamics During Fractional Flow in
662 Mixed-Wet Porous Media. *Water Resources Research*, *54*(5), 3277–3289.
663 https://doi.org/10.1029/2017WR022433